THE EFFECT OF ANGULAR STRUCTURE OF GAMMA-RAY BURST OUTFLOWS ON THE AFTERGLOW EMISSION

A. PANAITESCU AND P. KUMAR
Department of Astronomy, University of Texas, Austin, TX 78712

ABSTRACT

We investigate analytically the effect of an anisotropic distribution of the kinetic energy within a relativistic fireball on the decay of the afterglow emission, focusing on axially symmetric fireballs with a uniform core and a power-law decrease with angle outside the core. The afterglow fall-off steepens after the core becomes fully visible. For observer directions within the core, simple formulae are derived for the afterglow decay after the break, while for off-core observers results are shown graphically. Some criteria for assessing from observations the necessity of an angular structure and/or collimation are given. Applying them to several afterglows with light-curve breaks, we find that jets endowed with structure are required only if the circumburst medium has a wind-like (r^{-2}) stratification. Numerical fits to the multiwavelength emission of the afterglows 990510 and 000301c show that, for the former, the angular distribution of the ejecta kinetic energy is not far from uniformity, and that, with a standard power-law electron distribution, the sharp steepening of the R-band light-curve of the latter is better accommodated by a structured jet than an uniform outflow. Structured outflows may accommodate the shallower light-curve breaks observed in other afterglows.

Subject headings: gamma-rays: bursts - ISM: jets and outflows - methods: numerical - radiation mechanisms: non-thermal - shock waves

1. INTRODUCTION

Almost all the analysis of the decaying light-curves of Gamma-Ray Burst (GRB) afterglows is done within the framework of external shocks driven into the circumburst medium by ultrarelativistic ejecta (Mészáros & Rees 1997) whose kinetic energy is the same in all directions [1]. A non-isotropic distribution of the energy per solid angle within the outflow is a natural extension of the afterglow model. Fireballs whose kinetic energy and initial Lorentz factor fall-off with angle are power-laws have been considered for the first time by Mészáros, Rees & Wijers (1998), who studied the effect of such distributions on the afterglow light-curve decay. The faster dimming of the afterglow emission that a structured outflow can produce has been used by Dai & Gou (2001) to explain the steep fall-off of the optical light-curve of the afterglow 991208. Postnov, Prokhorov and Lipunov (2001) have suggested that GRB outflows may have a universal angular structure, the observed distribution of isotropic γ-ray outputs (which has a width of 3 dex) being due to the observer location. Rossi, Lazzati & Rees (2002) and Zhang & Mészáros (2002) have proposed that the light-curve breaks seen in several GRB afterglows and the narrow distributions of the GRB energy release (Frail et al. 2001) and jet kinetic energy (Panaitescu & Kumar 2002) may be due to the angular structure of fireballs.

In this work, we present an analytical treatment of the afterglow light-curves from structured fireballs (§2), focusing on axially symmetric fireballs endowed with a power-law distribution of the energy (§3). In §4.1 we give criteria which can be used to assess from the afterglow properties when structure and collimation of GRB outflows is required by observations, and apply these criteria to the afterglows whose optical light-curves exhibited a break. Section §4.2 presents the numerical modeling of two GRB afterglows, 990510 and 000301c, in the framework of structured jets, leading to a few important conclusions about the role of structure in these two cases.

2. SYNCHROTRON EMISSION FROM STRUCTURED FIREBALLS

In this section we calculate the evolution of the afterglow light-curve index $\alpha(t)$, defined as the logarithmic derivative with respect to the observer time t of the received flux F_ν (i.e. $F_\nu \propto t^{-\alpha}$) for a fireball endowed with structure. Our aim is to obtain the dependence of of $\alpha(t)$ and its asymptotic values at early and late times on the fireball's angular structure, i.e. the sharpness of the afterglow light-curve break that the structure can produce.

The calculation of the afterglow light-curve requires the following ingredients: dynamics of the fireball, spectrum of its emission, and integration over the equal photon-arrival-time surface. For analytical calculations, we shall ignore the tangential motions and mixing in the fireball and consider a simplified scenario where a fluid patch travels as if it were part of a uniform fireball.

For simplicity, in our analytical calculations of the light-curve index we consider only adiabatic GRB remnants, a case encountered when electrons acquire a negligible fraction of the post-shock energy or if they cool on a timescale longer than the dynamical time. Radiative losses could be important during the early afterglow, in which case the results presented in this section should be re-derived taking into account their effect on the evolution of the fireball Lorentz factor γ [eq. (1)]. This effect is included in the numerical calculations presented in §4.2.1 and §4.2.2.

For an adiabatic fireball, energy conservation gives that the Lorentz factor of a fluid patch moving in the direction (δ, ψ) (δ and ψ being the polar and azimuthal angles in a spherical polar coordinate system aligned to the direction toward the observer)

[1] Throughout this article, we use the term "uniform" to designate such outflows. If the angular distribution of the energy is not isotropic, the outflow will be called "structured". Tightly collimated outflows undergoing a significant lateral spreading at the time of observations will be referred to as "jets", while "fireballs" will be used if the lateral spreading is negligible.

decreases with its radial location r according to:

$$\gamma = K[\mathcal{E}(\delta,\psi)]^{1/2}\, r^{-(3-s)/2}\ , \tag{1}$$

where K is a constant, independent of direction, $\mathcal{E}$ is the kinetic energy per solid angle of the ejecta moving in the (δ,ψ) direction, and s describes the type of external medium: $n(r)\propto r^{-s}$, $s=0$ for a homogeneous medium and $s=2$ for a wind ejected at constant speed and mass-loss rate. Equation (1) holds for r larger than the radius at which the fireball deceleration sets in and until the fireball becomes semi-relativistic. Hereafter we will focus on this case, as it applies to observer times of at least 10 days, when the afterglow light-curve breaks are seen.

The photons emitted by a patch $(d\delta, d\psi)$ arrive at observer at a time t given by integrating

$$dt = dr(1-\beta\cos\delta)\ , \tag{2}$$

where β is the velocity of the patch, and the speed of light is unity. In the limit of relativistic motion ($\gamma\gg 1$) most radiation received by observer comes from the shocked medium moving at small angles ($\delta\ll 1$) relative to the line of sight. With these two assumptions, equation (2) leads to the following equation for the radius r of the patch moving in direction (δ,ψ) as a function of observer time

$$\frac{1}{2}r\delta^2 + \frac{1}{2(4-s)}\frac{r^{4-s}}{K^2\mathcal{E}} = t\ . \tag{3}$$

The peak synchrotron flux $F(\nu_p)$ received from a $(d\delta, d\psi)$ patch is proportional to $\mathcal{D}^3 I'(\nu'_p)d\Sigma$, where

$$\mathcal{D} = \frac{1}{\gamma(1-\beta\cos\delta)} \simeq \frac{2\gamma}{1+\gamma^2\delta^2} \tag{4}$$

is the Doppler boost factor, $I'(\nu'_p)$ is the comoving frame peak intensity at frequency $\nu'_p = \nu/\mathcal{D}(\delta)$ and $d\Sigma = r^2\sin\delta\, d\delta\, d\psi$ is the area of the patch. The $I'(\nu'_p)$ is proportional to the product $\mathcal{N}B$ of the surface density of energized electrons and the magnetic field within the shocked external medium. Therefore, the flux received at some frequency ν above the self-absorption frequency is

$$F_\nu(t) \propto \int_\Omega \frac{\gamma^3\mathcal{N}B\mathcal{F}(\nu)}{(1+\gamma^2\delta^2)^3}\ \delta\, d\delta\, d\psi \tag{5}$$

where the integral is over all directions of ejecta motion,

$$\mathcal{N} \propto r^{-2}\int_0^r n(r')r'^2 dr' \propto r^{1-s}\ , \tag{6}$$

$$B^2 \propto n\gamma^2 \propto r^{-s}\gamma^2\ , \tag{7}$$

assuming a magnetic energy density that is a constant fraction of the post-shock energy density, (which is the product the typical random Lorentz factor acquired by protons, γ, and the comoving proton density, $4n\gamma$), and the factor $\mathcal{F}(\nu)$ is the ratio of the flux at frequency ν to that at the peak ν_p. The time dependence of the flux given in equation (5) is due to the variation of γ, $\mathcal{N}$, and B with the location r of the patch, which is related to the observer time through equation (3). By substituting $\mathcal{N}$ and B in equation (5), the flux becomes

$$F_\nu(t) \propto \int_\Omega r^{-3+0.5s}\,(1+\gamma^2\delta^2)^{-3}\,\mathcal{E}^2\mathcal{F}(\nu)\ \delta\, d\delta\, d\psi\ . \tag{8}$$

The spectral factor $\mathcal{F}(\nu)$ is determined by the distribution of the radiating electrons. This distribution is shaped by the continuous injection in the downstream region of shock-accelerated electrons with a power-law distribution in energy, $dN_i/d\epsilon \propto \epsilon^{-p}$, above a minimum electron energy $\epsilon_i \propto \gamma$, and by radiative cooling. The resulting electron distribution exhibits a cooling break at an energy ϵ_c for which the cooling timescale ($\propto (\epsilon_c B^2)^{-1}$) equals the age of the fireball ($\propto r/\gamma$), therefore $\epsilon_c \propto \gamma/(rB^2)$. Above ϵ_c the effective electron distribution is $dN/d\epsilon \propto \epsilon^{-(p+1)}$ if $\epsilon_i < \epsilon_c$ (e.g. Kardashev 1962) or $dN/d\epsilon \propto \epsilon^{-2}$ if $\epsilon_c < \epsilon_i$. Consequently, the synchrotron spectrum is piecewise power-law, with breaks at the injection frequency $\nu_i \propto \mathcal{D}\epsilon_i^2 B$ and cooling frequency $\nu_c \propto \mathcal{D}\epsilon_c^2 B$:

$$\mathcal{F}(\nu) = \begin{cases} (\nu/\nu_i)^{1/3} & \nu < \nu_i \\ (\nu/\nu_i)^{-(p-1)/2} & \nu_i < \nu < \nu_c \end{cases}\ , \tag{9}$$

for $\epsilon_i > \epsilon_c$, while for $\epsilon_c < \epsilon_i$

$$\mathcal{F}(\nu) = \begin{cases} (\nu/\nu_c)^{1/3} & \nu < \nu_c \\ (\nu/\nu_c)^{-1/2} & \nu_c < \nu < \nu_i \end{cases}\ . \tag{10}$$

If ν is above both spectral breaks, then

$$\mathcal{F}(\nu) = (\nu/\nu_i)^{-p/2}(\nu_c/\nu_i)^{1/2}\ , \tag{11}$$

for either ordering of ν_i and ν_c. Thus, the time dependence of the factor $\mathcal{F}(\nu)$ is determined by those of the spectral breaks. After using equations (1) and (7), one obtains:

$$\nu_i \propto \frac{r^{-6+1.5s}\mathcal{E}^2}{1+\gamma^2\delta^2}\ ,\ \frac{\nu_c}{\nu_i} \propto \frac{r^4}{\mathcal{E}^2}\ . \tag{12}$$

For a given fireball structure $\mathcal{E}(\delta,\psi)$, one can calculate the afterglow light-curve $F_\nu(t)$ by integrating numerically equation (8) with r, γ, and $\mathcal{F}(\nu)$ corresponding to arrival time t and direction (δ,ψ) as given by equations (3), (1), (9)–(11), and (12). For now we simplify the integral in equation (8) by using an approximate solution to equation (3). In that equation, the second term in the left hand side is dominant for small δ, while the first term dominates at large δ. The two terms become equal for $r(\delta,\psi) = [(4-s)K^2\delta\mathcal{E}]$, which describes a curve $(\tilde\delta(\psi),\psi)$ on the equal photon arrival-time surface of time t given by

$$\mathcal{E}(\tilde\delta,\psi)\tilde\delta^{2(4-s)} = \frac{t^{3-s}}{(4-s)K^2}\ . \tag{13}$$

From equation (1), the above expression for r shows that $\tilde\delta(\psi)$ also satisfies $\tilde\delta(\psi)\,\gamma(\tilde\delta,\psi) = (4-s)^{-1/2}$.

For $\delta < \tilde\delta(\psi)$, equations (1) and (3) give

$$r \propto (\mathcal{E}t)^{1/(4-s)}\ ,\ \ \gamma \propto (\mathcal{E}t^{s-3})^{1/2(4-s)}\ , \tag{14}$$

while for $\tilde\delta(\psi) < \delta$

$$r \propto t/\delta^2\ ,\ \ \gamma \propto \delta^{3-s}(\mathcal{E}t^{s-3})^{1/2}\ . \tag{15}$$

The integral in equation (8) can then be approximated as the sum of an "inner" integral over the $\delta < \tilde\delta(\psi)$ disk, where r and γ are given by equation (14), and an "outer" integral over directions outside this disk, where r and γ are given by equation

(15). It can be shown by numerical integration that these two integrals have the same time dependence, thus the calculation of the afterglow light-curve can be simplified by retaining only the inner integral. The product $\gamma\delta$ increases with δ, thus its maximal value on the inner disk is $\tilde{\delta}\gamma(\tilde{\delta},\psi) = (4-s)^{-1/2} < 1$, therefore the factor $(1+\gamma^2\delta^2)^{-3}$ in equation (8) is approximately unity. With these simplifications, the afterglow flux becomes:

$$F_\nu \propto t^{(0.5s-3)/(4-s)} \int_0^{2\pi} d\psi \int_0^{\tilde{\delta}(t,\psi)} d\delta\ \delta\, \mathcal{E}^{(5-1.5s)/(4-s)}\, \mathcal{F}(\nu)\ , \tag{16}$$

where $\mathcal{F}(\nu)$ is given by equations (9)–(11) with

$$\frac{\nu}{\nu_i} \propto \mathcal{E}^{-1/2} t^{3/2}\ ,\ \frac{\nu_c}{\nu_i} \propto \left(\mathcal{E}^{s-2}t^2\right)^{2/(4-s)}\ . \tag{17}$$

Therefore the afterglow light-curve has the form

$$F_\nu(t) \propto t^{f(p,s)} \int_0^{2\pi} d\psi \int_0^{\tilde{\delta}(t,\psi)} d\delta\ \delta\, [\mathcal{E}(\delta,\psi)]^{g(p,s)}\ , \tag{18}$$

where the exponents f and g depend on the electron index p and type of external medium.

3. POWER-LAW FIREBALLS

Hereafter we shall consider fireballs whose kinetic energy per solid angle $\mathcal{E}$ is axially symmetric, uniform within a core of size θ_c, and a power-law outside it [2] :

$$\mathcal{E}(\theta) = \mathcal{E}_0 \times \begin{cases} 1 & \theta < \theta_c \\ (\theta/\theta_c)^{-q} & \theta_c < \theta \end{cases}\ , \tag{19}$$

where $q > 0$ and the angle θ measured from the symmetry axis of the fireball is related to the direction (δ,ψ) through a rotation:

$$\cos\theta = \cos\delta\, \cos\theta_{obs} - \sin\delta\, \cos\psi\, \sin\theta_{obs}\ , \tag{20}$$

θ_{obs} being the angle between the observer's line toward the fireball center and the fireball symmetry axis.

3.1. *Observers within the Fireball Core: Analytical Results*

As shown by Granot et al. (2002), the emission from the uniform core depends very weakly on the observer location. The emission received from outside the fireball core should depend even less on the observer's off-set θ_{obs}, thus, to a good approximation, we can consider $\theta_{obs} = 0$. Then equation (13) gives

$$\tilde{\delta}(t) \propto \begin{cases} t^{(3-s)/2(4-s)} & \text{if } \tilde{\delta} < \theta_c \\ t^{(3-s)/[2(4-s)-q]} & \text{if } \theta_c < \tilde{\delta} \end{cases}\ . \tag{21}$$

At early times, when $\tilde{\delta} < \theta_c$, the afterglow emission arises from within the uniform fireball core. In this case, the afterglow light-curve is $F_\nu \propto t^{f(p,s)} \int_0^{\tilde{\delta}(t)} d\delta\, \delta \propto t^{f(p,s)} \tilde{\delta}^2$, which leads to $F_\nu \propto t^{-\alpha_1}$ with

$$\alpha_1 = \begin{cases} (3p-3)/4 & s=0\ \&\ \nu_i < \nu < \nu_c \\ (3p-2)/4 & s=0,2\ \&\ \max\{\nu_i,\nu_c\} < \nu \\ (3p-1)/4 & s=2\ \&\ \nu_i < \nu < \nu_c \end{cases}\ . \tag{22}$$

These are the usual results for a uniform fireball.

At late times, when $\tilde{\delta} > \theta_c$, the contribution of the ejecta outside the core to the afterglow emission is proportional to

$$\int_{\theta_c}^{\tilde{\delta}(t)} \delta^{1-qg(p,s)} d\delta = (2-qg)^{-1} \left(\tilde{\delta}^{2-qg} - \theta_c^{2-qg}\right)\ . \tag{23}$$

If $qg(p,s) < 2$, then the first term in the right hand side dominates, while for $qg(p,s) > 2$, the last term is the largest and has the same time dependence as the emission from the fireball core. Using the expression of $g(p,s)$ for each case, the transition value of the structural parameter is

$$\tilde{q} = \begin{cases} \frac{8}{p+4} & (s=0,\nu_i<\nu<\nu_c)\ \text{or}\ (s=2,\max\{\nu_i,\nu_c\}<\nu) \\ \frac{8}{p+3} & (s=0,\max\{\nu_i,\nu_c\}<\nu)\ \text{or}\ (s=2,\nu_i<\nu<\nu_c) \end{cases}\ . \tag{24}$$

For $q < \tilde{q}$, the fall-off of $\mathcal{E}(\theta)$ is sufficiently shallow that the emission from the ejecta outside the core is dominant, the afterglow light-curve $F_\nu \propto t^{f(p,s)}\tilde{\delta}^{2-qg}$ decaying as $F_\nu \propto t^{-\alpha_2}$ with

$$(s=0)\quad \alpha_2 = \frac{1}{4-\frac{1}{2}q} \times \begin{cases} 3p-3+\frac{3}{2}q & \nu_i<\nu<\nu_c \\ 3p-2+q & \max\{\nu_i,\nu_c\}<\nu \end{cases}\ , \tag{25}$$

for a homogeneous medium and

$$(s=2)\ \ \alpha_2 = \frac{1}{4-q} \times \begin{cases} 3p-1-\frac{1}{2}q(p-1) & \nu_i<\nu<\nu_c \\ 3p-2-\frac{1}{2}q(p-2) & \max\{\nu_i,\nu_c\}<\nu \end{cases}\ , \tag{26}$$

for a wind-like medium. For $q > \tilde{q}$, $\mathcal{E}(\theta)$ decreases sufficiently fast away from the fireball axis that the afterglow emission is dominated by the uniform core and/or by the ejecta just outside the core. In either case, the afterglow light-curve $F_\nu \propto t^{f(p,s)}\theta_c^{2-qg}$ decays as $F_\nu \propto t^{-\alpha_2}$ with

$$\alpha_2 = \begin{cases} 3p/4 & (s=0,\nu_i<\nu<\nu_c)\ \text{or}\ (s=2,\max\{\nu_i,\nu_c\}<\nu) \\ \frac{3p+1}{4} & (s=0,\max\{\nu_i,\nu_c\}<\nu)\ \text{or}\ (s=2,\nu_i<\nu<\nu_c) \end{cases} \tag{27}$$

Taking into account that for most well-observed afterglows, the electron index is between 1.5 and 2.5, it follows that $5/4 \lesssim \tilde{q} < 7/4$. Therefore, for fireballs that do not undergo significant lateral spreading at the observing time, the asymptotic index α_2 of the afterglow light-curve is independent of the fireball power-law structure if $q \gtrsim 2$. This is true also for observers located outside the fireball core (§3.3), at times when the core is visible. [3]

Equations (22) and (25)–(27) allow the calculation of the steepening of the light-curve index $\Delta\alpha = \alpha_2 - \alpha_1$ produced by the passage of the cooling frequency ν_c through the observing band or by the core edge becoming visible. For the former, $\Delta\alpha = 1/4$ either if the entire visible region of the fireball is within its core or if the core edge is observable but $q > \tilde{q}$. For

[2] Other types of structure can be considered as well, but power-laws allow sufficient flexibility with a minimal number of new parameters

[3] A decelerating, point-like source moving at Lorentz factor γ and at an angle δ relative to the direction toward the observer, becomes visible when $\gamma\delta = 1$, i.e. when the cone of its relativistically beamed emission starts to contain the direction toward the observer

$q < \tilde{q}$, the passage of ν_c (which decreases in time for a homogeneous medium, but increases if the medium is wind-like) yields $\Delta\alpha = (2-q)/(8-q) < 1/4$.

Because $\gamma\delta$ increases with δ and $\tilde{\delta}\,\gamma(\tilde{\delta}) = (4-s)^{-1/2} < 1$, when the core edge becomes visible ($\gamma(t_c,\theta_c)\theta_c = 1$) the core edge is outside the inner disk ($\theta_c > \tilde{\delta}(t_c)$). Therefore $\gamma(t_c,\theta_c)$ satisfies equation (15), which, together with $\gamma(t_c,\theta_c) = \theta_c^{-1}$, yields

$$t_c \propto [\mathcal{E}_0\theta_c^{2(4-s)}]^{1/(3-s)} \ . \tag{28}$$

For $q > \tilde{q}$ the light-curve break across t_c is $\Delta\alpha = 3/4$ for a homogeneous medium and $\Delta\alpha = 1/2$ for a wind, while for $q < \tilde{q}$ the break is

$$\Delta\alpha = \begin{cases} \dfrac{3q(8/\tilde{q}-1)}{4(8-q)} < 3/4 & s = 0 \\ \dfrac{q(4/\tilde{q}-1)}{2(4-q)} < 1/2 & s = 2 \end{cases} \ . \tag{29}$$

Therefore the maximal light-curve break that a non-spreading, power-law fireball can yield to an observer located with its uniform core is $3/4$ for a homogeneous medium and $1/2$ for a wind (Panaitescu, Mészáros & Rees 1998).

3.2. *Observers within the Fireball Core: Numerical Results*

The evolution of the light-curve index $\alpha(t)$, obtained by calculating numerically the integral of equation (8) (i.e. without the simplifications made subsequently), for an on-axis observer is shown in Figure 1 for some values of the structural parameter q. Before the edge core becomes visible, the index $\alpha = \alpha_1$ given by equation (22). When the core edge becomes visible, at $t = t_c \sim 2\times10^3\,t_d$ for $s = 0$ and $\sim 4\times10^3\,t_d$ for $s = 2$ (t_d being the observer frame deceleration timescale for the fluid moving toward the observer: $\theta = 0$), the index α increases toward the α_2 given in equations (25) and (26) for $q = 1 < \tilde{q}$ and that given in equation (27) for $q = 2,3 > \tilde{q}$. As shown in Figure 1, 80% of the light-curve decay steepening across t_c lasts a factor 4–6 in time for $s = 0$ and a factor 7–10 for $s = 2$. The slower transition for a wind-like medium is caused by the slower decrease of the fireball Lorentz factor with time, given in equations (14) and (15): for $s = 0$, $\gamma \propto t^{-3/8}$ if $\delta < \tilde{\delta}$ and $\gamma \propto t^{-3/2}$ if $\delta > \tilde{\delta}$, while for $s = 2$, $\gamma \propto t^{-1/4}$ and $\gamma \propto t^{-1/2}$, respectively. The fireball deceleration being slower for a wind-like medium, it takes a longer time for the core edge to become fully visible, thus the transition between the asymptotic light-curve indices is smoother.

Figure 1 also shows the light-curve steepening for a fireball with $q = \infty$, corresponding to a uniform, collimated outflow with a sharp edge, undergoing lateral spreading. Due to the widening of the jet aperture, $\alpha(t < t_c)$ is not constant, but increases slowly in time. Furthermore, $\alpha(t \gg t_c)$ is larger than without lateral spreading, reaching $\alpha_2 = p$ (Rhoads 1999). For a uniform, spreading jet, interacting with a homogeneous medium, the fastest 70% of the analytically expected steepening $\Delta\alpha = p - \alpha_1$ is acquired over a factor 20 in time if $\nu < \nu_c$ and 10 if $\nu_c < \nu$, while for a wind-like medium the corresponding factors are 100 and 1,000, respectively. Therefore the "jet-break" transition is significantly slower and smoother if the surrounding medium is the wind that a massive GRB progenitor expelled before the burst (Kumar & Panaitescu 2000).

3.3. *Observers outside the Fireball Core*

For observers located outside the uniform fireball core, the pre-break light-curve fall-off is mitigated as the more energetic ejecta located closer to the fireball axis become visible, therefore the early time light-curve index α_1 decreases in time (see also the light-curves presented by Granot & Kumar 2003 and Wei & Jin 2003). The fireball axis is seen at a time satisfying

$$t_a \propto [\mathcal{E}_0\theta_{obs}^{2(4-s)}]^{1/(3-s)} \ , \tag{30}$$

similar to the time t_c when the core edge becomes visible to an on-axis observer (eq. [28]) but with the core size θ_c replaced by the angle θ_{obs} between the fireball axis and the center – observer line (Rossi, Lazzati & Rees 2002). Well after t_a, when the beaming factor $\mathcal{D}$ is almost the same across the fireball core, the light-curve index for an off-core observer should reach that given in equations (25)–(27) for an on-axis observer. Thus, the flattening of the light-curve fall-off at $t < t_a$ yields larger light-curve breaks $\Delta\alpha$ than for an on-axis observer. This is the most important feature arising from the structure of the outflow.

Figure 2 shows the evolution of α obtained from equation (8) for an off-core observer located at $\theta_{obs} = 3\theta_c$. As can be noticed, a stronger fall-off of the ejecta energy away from the fireball axis (i.e. a larger parameter q), leads to a more prominent flattening of the afterglow light-curve at $t < t_a$, where $t_a \sim 3\times10^3\,t_d(\theta = 0)$ for $s = 0$ and $\sim 10^5\,t_d(\theta = 0)$ for $s = 2$. Also as expected, at $t \gg t_a$ the index α asymptotically reaches the values for an on-axis observer. Note that, for the same parameter q, the light-curve break $\Delta\alpha$ across t_a is larger for a homogeneous medium, and that the transition between the lowest value of α and the α_2 at late time takes about a decade in time for a homogeneous medium and about two decades for a wind-like medium. The slow transition in the latter case (see also Dai & Gou 2001 and Granot & Kumar 2003) suggests that, for a wind-like stratified medium, light-curve breaks arising from the structure of the outflow may be too shallow compared the light-curve steepenings observed in some afterglows, which last less than a decade in time.

The minimal value α_{min} reached by the light-curve index before the break depends not only on the structural parameter q, as shown in Figure 2, but also on the location of the observer, through the ratio θ_{obs}/θ_c, and on the slope p of the electron distribution. As illustrated in Figure 3, the observer location has a much stronger effect on the sharpness of the light-curve break produced by the fireball structure if the external medium is homogeneous. In this case, for observer directions further away from the fireball axis, α_{min} decreases and the transition between α_{min} and the α_2 at late times lasts shorter (relative to the break-time t_a), the light-curve break becoming sharper. Consequently, for a homogeneous medium, higher observer offsets will accommodate easier some of the observed sharp breaks. However, given the expected correlation between the GRB peak flux and the energy of ejecta moving toward the observer, large observer offsets render the burst less likely to be detected. Furthermore, for homogeneous media, as shown in Figure 3, large offsets also yield pre-break light-curve indices that are too small compared to those observed. Taking $\theta_{obs}/\theta_c = 3$ as a more likely case, so that the resulting GRB is sufficiently bright and the afterglow break sufficiently sharp, we show in Figure 4 the dependence of the pre-break minimum light-curve index α_{min} on the structural parameter q and on the electron index p. Because most of the effect of the latter is through the $3p/4$ fac-

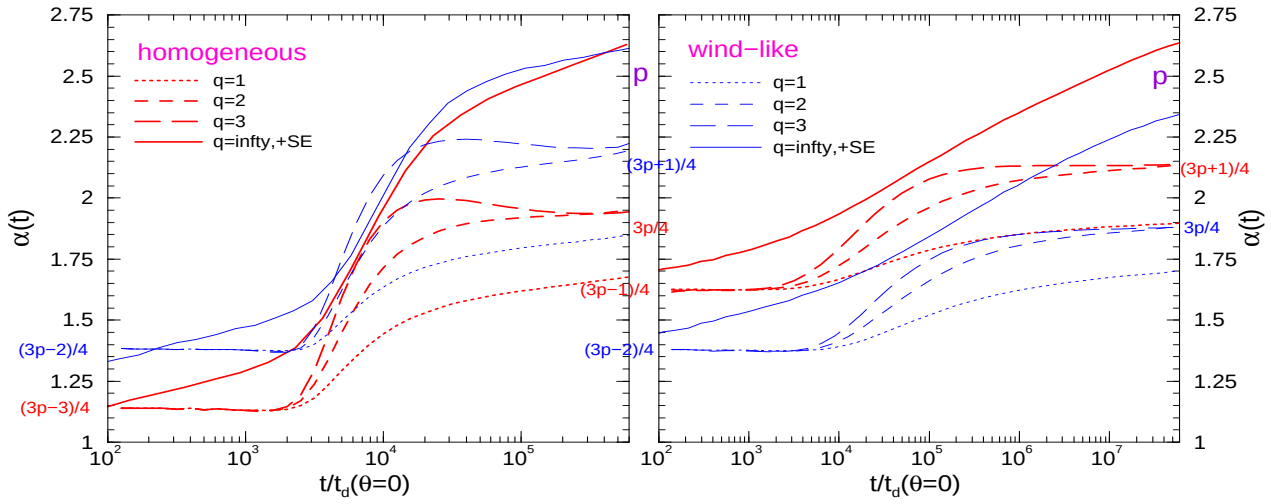

FIG. 1.— Evolution of the logarithmic derivative $\alpha = -(d \ln F_\nu / d \ln t)$ of the afterglow synchrotron flux at frequencies below (*thick lines*) and above the cooling frequency (*thin lines*), for homogeneous (*left panel*) and wind-like circumburst media (*right panel*), and for a power-law angular distribution of the kinetic energy per solid angle of the ejecta $\mathcal{E}$ with angle θ off the symmetry axis of the fireball – $\mathcal{E}(\theta) \propto \theta^{-q}$ – outside a core of uniform density. Solid curves are for a uniform jet with sharp boundaries (corresponding to $q = \infty$) and undergoing sideways expansion. The observer is placed on the fireball axis, time being measured in deceleration timescales for the ejecta moving along the fireball axis. When the fireball has decelerated enough that the edge of its core becomes visible, α increases and the afterglow light-curve exhibits a break. The electron distribution is assumed to be a power-law of exponent $-p$ with $p = 2.5$. The asymptotic indices expected at early and late times are indicated on the abscissa. Note the faster transition between the asymptotic indices in the case of a homogeneous medium and that, for $q \geq 2$, the post-break index is independent of q, as the afterglow emission arises mostly from the fireball core.

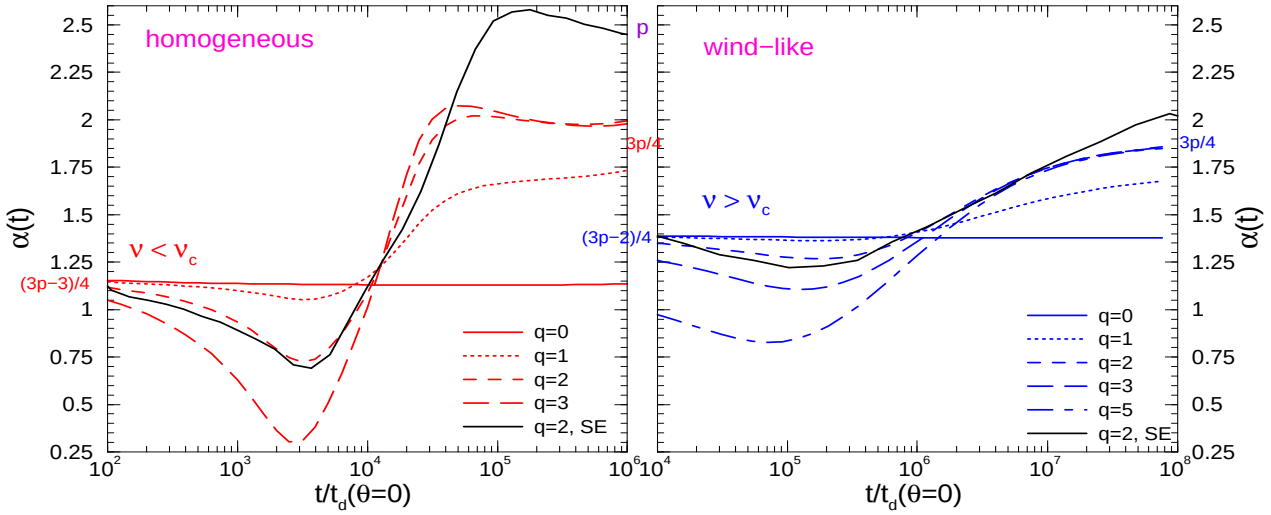

FIG. 2.— Evolution of the light-curve index α for various parameters q for the power-law fireball structure and for an observer located at angle $\theta_{obs} = 3\,\theta_c$ relative to the fireball symmetry axis, θ_c being the angular size of the uniform core. The electron distribution parameter is $p = 2.5$. When the fireball core becomes visible, α has a minimal value which depends on q and on the ratio θ_{obs}/θ_c (Figure 3). Note the slower evolution of α for a wind-like medium (*right panel*) and the weaker effect that the structure has on α in this case. For the remaining cases ($\nu > \nu_c$ and homogeneous medium, $\nu < \nu_c$ and wind-like medium), the evolution of α is similar, the curves being shifted upward by 1/4. The continuous black line is for a jet of initial opening $\Theta_0 = 3\theta_c$, (i.e. the observer is located on the jet edge at $t = 0$) and for $q = 2$.

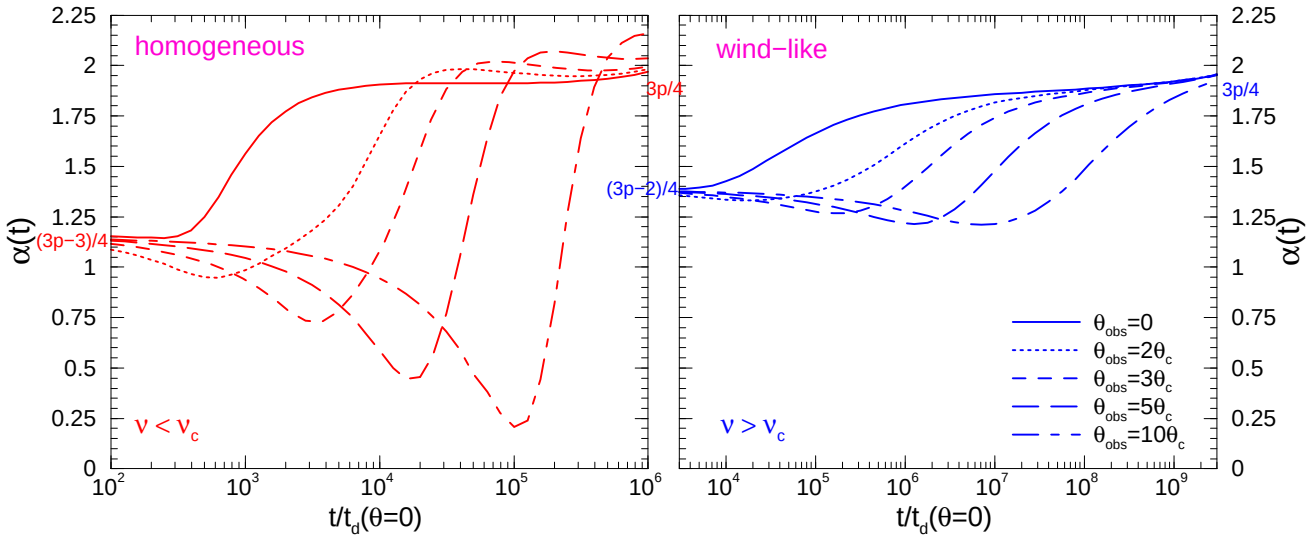

FIG. 3.— Same as in Figure 2 but for a fixed parameter $q = 2$ and various ratios θ_{obs}/θ_c. The line coding is the same for both panels. Note that observers located further away from the fireball symmetry axis will see a stronger flattening of the afterglow light-curve followed by a sharper break, and that the break is shallower for a wind-like medium (*right panel*).

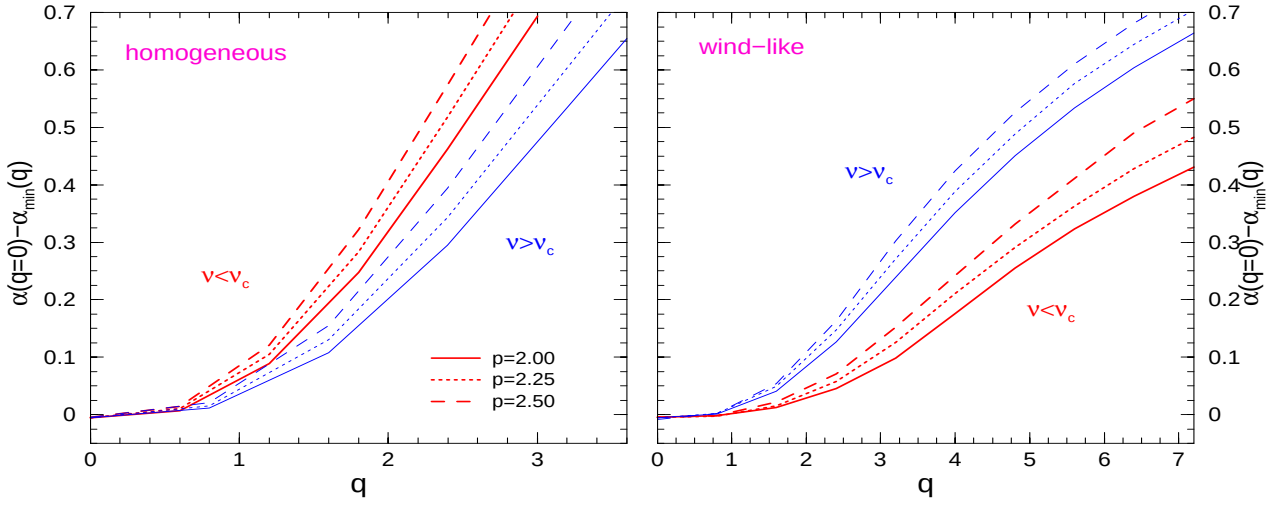

FIG. 4.— Effect of fireball structure (parameterized by q) on the minimum light-curve index α_{min} reached before the break, for some values of the electron index p. The observer location is $\theta_{obs} = 3\theta_c$. *Thick curves* are for $\nu < \nu_c$ while *thin lines* indicate $\nu > \nu_c$. Most of the dependence of α_{min} on p has been eliminated by shifting vertically the curves by the $\alpha(q = 0)$ expected for a uniform fireball. Note the stronger flattening (i.e. decrease of α_{min}) that a homogeneous medium (*left panel*) yields for the same structural parameter q.

tor in equation (22), the $\alpha_{min}(q)$ has been offset by its value $\alpha_{min}(q=0)$ for a uniform fireball, to illustrate the less trivial effect of p on α_{min}.

4. STRUCTURED FIREBALLS/JETS AND AFTERGLOW OBSERVATIONS

The minimum light-curve index α_{min} shown in Figure 2 should be close to the pre-break index usually inferred by fitting the afterglow light-curve with a smoothed broken power-law (e.g. Beuermann et al. 1999), while the post-break index inferred from observations is either the α_2 given in equations (25)–(27) for a structured fireball, or the electron index p for a jet (uniform or with structure) whose edge is visible. Furthermore, one can determine from multiband optical observations the afterglow intrinsic spectral slope β_o, defined as $F_\nu \propto \nu^{-\beta_o}$, which depends only on the electron index p:

$$\beta_o = \begin{cases} (p-1)/2 & \nu_i < \nu_o < \nu_c \\ p/2 & \max\{\nu_i,\nu_c\} < \nu_o \end{cases} . \quad (31)$$

If there is a significant dust reddening in the host galaxy, β_o can be determined with the aid of the X-ray spectral slope, if available, or of fits to the optical spectrum, if it is sufficiently curved to constrain the host extinction for an assumed dust-reddening law (e.g. Jensen et al. 2001, Fynbo et al. 2001). Thus, observations provide three characteristics of the afterglow emission: pre- and post- break light-curve indices α_{min} and α_2, and spectral slope β_o, which constrain three major fireball parameters: the structural index q, the observer location θ_{obs}/θ_c, and the electron index p.

An analytical determination of q from the measured asymptotic light-curve indices is hampered by the complicated dependence of the pre-break index α_{min} on q and observer location (Figures 2 and 3) and by that the post-break index α_2 could be affected by the lateral spreading of the outflow. The observer location $\theta_{obs} = 3\,\theta_c$ considered in Figures 2 and 4 can be taken as representative, but, for a more secure approach to determining the fireball structure, one should fit the observed break with a numerically calculated afterglow light-curve, allowing for a free observer location. Before proceeding on this path, we discuss below how the observed asymptotic light-curve indices α_1 and α_2 and the spectral slope β_o can be used to assess if a structured fireball is required by the observations and if the lateral spreading of the outflow is significant.

4.1. *How to Constrain the Outflow Collimation and Structure Using Observations*

We make here the *assumption* that the asymptotic pre- and post-break light-curve indices are determined only by the fireball/jet angular structure, radial distribution of the external medium density, and slope of the shock-accelerated electron distribution. In principle there could be other factors that determine these indices, such as: a refreshed shock produced by slower ejecta catching-up with the GRB remnant (Panaitescu, Mészáros & Rees 1998), which may mitigate the afterglow dimming rate if sufficient energy is injected, or a dependence on the ejecta Lorentz factor of the electron distribution index or fractional energy acquired by electrons or magnetic field.

From equations (22) and (31) it follows that, for a uniform outflow, the pre-break light-curve index is

$$\alpha_1 = \frac{3}{2}\beta_o + \begin{cases} 0 & s=0 \ \&\ \nu_i < \nu_o < \nu_c \\ -1/2 & s=0,2 \ \&\ \max\{\nu_i,\nu_c\} < \nu_o \\ 1/2 & s=2 \ \&\ \nu_i < \nu_o < \nu_c \end{cases} . \quad (32)$$

Thus, *if the observed α_1 is smaller than given above, a structured outflow is required* (1^{st} criterion), as well as an off-core observer location. Given that for a fireball with a decreasing $\mathcal{E}(\theta)$, the post-break light-curve index α_2 cannot exceed the values given in equation (27), *if the observed α_2 exceeds*

$$\alpha_2 = \frac{3}{2}\beta_o + \begin{cases} 3/4 & s=0 \ \&\ \nu_i < \nu_o < \nu_c \\ 1/4 & s=0 \ \&\ \max\{\nu_i,\nu_c\} < \nu_o \\ 1 & s=2 \ \&\ \nu_i < \nu_o < \nu_c \\ 0 & s=2 \ \&\ \max\{\nu_i,\nu_c\} < \nu_o \end{cases} , \quad (33)$$

then a highly collimated outflow (jet), whose boundary becomes visible when the light-curve break is observed, *is required* (2^{nd} criterion). In this case, the post-break light-curve index reaches its maximal value: $\alpha_{max} = p$. From equation (31), it follows that

$$\alpha_{max} = \begin{cases} 2\beta_o + 1 & \nu_i < \nu_o < \nu_c \\ 2\beta_o & \max\{\nu_i,\nu_c\} < \nu_o \end{cases} . \quad (34)$$

Combining equations (32) and (34), the maximum steepening $\Delta\alpha = \alpha_2 - \alpha_1$ that a uniform jet can produce is

$$\Delta\alpha = \frac{1}{2}\beta_o + \begin{cases} 1 & s=0 \ \&\ \nu_i < \nu_o < \nu_c \\ 1/2 & (s=0 \ \&\ \max\{\nu_i,\nu_c\} < \nu_o) \ \text{or} \ s=2 \end{cases} . \quad (35)$$

Thus, *if the observed $\Delta\alpha$ exceeds the above value, a structured jet is required* (3^{rd} criterion). However, *if the observed α_2 exceeds that given in equation (34)*, then the light-curve break cannot be due entirely to the collimation of the ejecta, and *another mechanism for light-curve breaks*, such as a spectral break passing through the observing band, *is required* (4^{th} criterion). This passage will also produce a color change (i.e. β_o increases) and an achromatic light-curve break.

Applying the above criteria to the optical emission of afterglows with light-curve breaks, it is possible to identify the cases where structured fireballs or jets are required:

i) from the 1^{st} criterion, angular structured is required by the pre-break index α_1 of the afterglows
- a) 980519, 990510, and 991216, if $s = 2$,
- b) 000301c and 010222, if $\nu_o < \nu_c$,
- c) 990123 and 000926, if $s = 2$ and $\nu_o < \nu_c$,

ii) from the 2^{nd} criterion, a jet undergoing lateral spreading is required by the post-break index α_2 of the afterglows
- a) 990510,
- b) 990123, 000926, and 010222, if $\nu_c < \nu_o$,
- c) 991208 if $\nu_o < \nu_c$,

iii) from the 3^{rd} criterion, a structured jet is required by the steepening $\Delta\alpha$ observed for the afterglow 990510, if $s = 2$,

iv) from the 4^{th} criterion, the passage of a spectral feature through the optical domain is required (Li & Chevalier 2001, Panaitescu & Kumar 2002) by the steep post-break index α_2 of the afterglows 991208 and 000301c, if $\nu_c < \nu_o$ and, perhaps, by 000301c if $\nu_o < \nu_c$.

4.2. *Numerical Modeling of Structured Jets*

Equations (32)–(35) allow one to assess if a structured outflow is necessary or sufficient to explain the pre and post-break

optical light-curve indices. A more conclusive test should investigate if the light-curve steepening produced by a structured fireball is as sharp as observed, and if the fireball emission at different wavelengths is consistent with the observations. For uniform outflows, the latter is usually done using a snapshot broadband afterglow spectrum, but, for structured outflows, one has to take in account that, at the same observer time, the ejecta moving at different angles have different Lorentz factors, thus their synchrotron emissions have with different characteristic frequencies.

To perform such a test, the data should be fit numerically, followed by a comparison of the best fit χ^2 obtained for the various model features that are investigated. The model used hereafter takes into account the spread in the photon arrival time and Doppler boost due to the curvature of the jet surface, radiative losses, the effect of inverse Compton scatterings on the cooling frequency, and the self-absorption and interstellar scintillation at radio frequencies. The uniform jet expands sideways at a comoving frame tangential velocity equal to the sound speed c_s. Thus, the jet opening Θ is given by

$$d\Theta(r) = \frac{c_s}{r} dt' = \frac{c_s}{r\gamma}\, dr \ , \tag{36}$$

where t' is time measured in the comoving frame. The uniformity of the jet is assumed to be maintained during the jet lateral spreading. The variation of the energy per solid angle $\mathcal{E}$ of an infinitesimal ring $(\theta, \theta + \delta\theta)$ during dt' is $d\mathcal{E} = -\mathcal{E}\, d(\delta\theta)/\delta\theta$, where $d(\delta\theta)$ is the spreading of the ring during dt'. Therefore, the assumption of jet uniformity at any time is equivalent to that $d(\delta\theta)/\delta\theta$ is a θ-independent quantity. Then, from equation (36), it follows that the spreading of any infinitesimal ring is assumed to be governed by

$$d(\delta\theta) = \frac{\delta\theta}{\Theta} \frac{c_s}{r\gamma}\, dr \ . \tag{37}$$

The collimation of ejecta affects the afterglow emission in three ways. First, the size of the visible part of the jet (r/γ) stops increasing when $\gamma\Theta = 1$, i.e. when the edge is seen, yielding a light-curve steepening (Panaitescu, Mészáros & Rees 1998). Second, the sideways expansion of the jet increases its sweeping area, which alters the jet dynamics (Rhoads 1999). Third, the lateral spreading decreases the surface density of the swept-up medium, moving a fraction of the radiating electrons outside the visible region when the jet edge is not yet seen. The last two effects are important when $\Theta - \Theta_0 \gtrsim \Theta_0$ (Θ_0 being the initial jet opening), which, with the aid of equations (1) and (36), can be shown to occur slightly *after* the radius where the jet edge becomes visible if the external medium is homogeneous, and slightly *before* if the medium is wind-like. The jet lateral spreading contributes to the light-curve steepening caused by seeing the jet edge, but also delays the completion of the steepening. Because of the slower deceleration caused by a wind-like medium, this completion lasts longer for $s = 2$ than for $s = 0$. Therefore, the light-curve breaks for spreading jets should be smoother than for structured fireballs, the effect being stronger for a wind-like medium than for a homogeneous one (Figures 1 and 2).

For a structured fireball, we divide its surface in $(\theta_i, \theta_i + \delta\theta_i)$ rings and calculate the ring location ($\theta_i(r)$) and width ($\delta\theta_i(r)$) using equation (37), with the local sound speed $c_s(\theta_i)$ obtained from the shock jump conditions and dynamics ($\gamma_i(r)$) of the ring, and with $\Theta(r) = \sum_i \delta\theta_i(r)$. For each step $r \to r + dr$, the deceleration of the ring is calculated as if it were part of a uniform fireball of kinetic energy per solid angle $\mathcal{E}(\theta_i)$, which is adjusted at each step to account for the ring spreading $\delta\theta_i(r)$ and radiative losses. Therefore, we ignore any fluid mixing expected to arise from the tangential flow, a factor which Granot & Kumar (2003) have found to have a weak effect on the afterglow emission. Equation (37) provides a simple one-to-one mapping of the jet structure at radius r into that at $r + dr$, and maintains computationally inexpensive the numerical algorithm for the dynamics.

The uniform jet model has six free parameters: the initial energy density per solid angle within the ejecta $\mathcal{E}$, the jet initial half-opening Θ_0, the external particle density n (or the parameter A_* introduced by Chevalier & Li 1999 for an r^{-2} wind profile), the exponent p of the electron distribution, and the fractional energies in electrons and magnetic field in the post-shock gas. For observers located within the initial jet opening (which is a condition for seeing a GRB), this location is irrelevant (Granot et al. 2002). The structured jet model with a power-law distribution of the energy per solid angle has three additional parameters: the core size θ_c, the power-law exponent q, and the observer location θ_{obs}.

We apply the structured jet model to the two afterglows with the largest observed steepening $\Delta\alpha$: 990510 and 000301c. For 990510, a jet undergoing lateral spreading at the time of observations is required for either type of external medium. The purpose of modeling this afterglow is twofold: for $s = 0$ we will determine how much structure is allowed by the pre-break light-curve index, for $s = 2$ we will assess if a structured outflow improves significantly the best fit by sharpening the light-curve steepening. The latter is also the purpose of modeling the afterglow 000301c with a structured jet, as its sharp light-curve break cannot reproduced with a uniform jet and standard electron distribution even if the external medium is homogeneous.

4.2.1. *GRB 990510*

The optical emission of the 990510 afterglow exhibited a break from an index $\alpha_1 = 0.82 \pm 0.02$ to $\alpha_2 = 2.18 \pm 0.05$ (Harrison et al. 1999) at $t \sim 2$ days (see Figure 6). The optical and X-ray slopes, $\beta_o = 0.61 \pm 0.12$ (Stanek et al. 1999) and $\beta_x = 1.03 \pm 0.08$ (Kuulkers et al. 2000), indicate that $\nu_o < \nu_c < \nu_x$.

In the framework of uniform jets, we have previously found (Panaitescu & Kumar 2002) that the optical light-curve steepening can be well accommodated ($\chi^2 = 36$ for 69 degrees of freedom) with a jet of initial kinetic energy $E_0 = (1 \div 6) \times 10^{50}$ ergs, initial opening $\Theta_0 \simeq 3\,\mathrm{deg}$, interacting with a homogeneous medium of density $n = 0.1 \div 0.4\,\mathrm{cm}^{-3}$. We have also found that a wind-like medium cannot reproduce the steepness of the optical light-curve break, yielding an unacceptable best fit ($\chi^2 = 127$ for 69 df).

For a *homogeneous* external medium, equation (32) shows that $\alpha_1 = 0.92 \pm 0.18$ for a uniform outflow, which is consistent with the observed index, thus a large structural parameter q is disfavored, otherwise the early decay would be too shallow. Further, equation (33) shows that, for a fireball, the post-break index α_2 cannot exceed 1.67 ± 0.18, which is too small compared to that observed, thus a spreading jet is required. In this case, equation (34) leads to a post-break index $\alpha_2 = 2.22 \pm 0.24$, which is consistent with the measured index. The above conclusion that the pre-break light-curve index of the afterglow of GRB 990510 does not allow much structure in a spreading jet is illustrated in Figure 5, showing the χ^2 of the fits

obtained for several combinations of the structural parameter q and jet core size-to-opening ratio θ_c/Θ_0, and for two particular observer locations: the jet axis and the jet edge. By decreasing the θ_c/Θ_0 ratio or increasing q, a stronger jet structure is enforced. As can be noticed, only jets with $\theta_c \gtrsim 0.2\,\Theta_0$ for $q = 1$ and $\theta_c \gtrsim 0.3\,\Theta_0$ for $q \geq 2$ provide acceptable fits (defined by a probability larger than 10%), while fits as good as that provided by a uniform jet ($\chi^2 = 36$) require that $\theta_c \gtrsim 0.3\,\Theta_0$ if $q = 1$ and $\theta_c \gtrsim 0.4\,\Theta_0$ if $q = 2$. Thus, for $s = 0$, the afterglow of GRB 990510 is best explained by a structured jet with a variation of the energy per solid angle less than a factor ~ 5 across the jet surface. The radio, optical and X-ray light-curves for the best fit obtained with a structured jet are shown in the left panel of Figure 6. We note that its parameters are similar to those for a uniform jet.

For a *wind-like* external medium, equation (32) gives $\alpha_1 = 1.42 \pm 0.18$ for a uniform outflow, thus structure is required in this case to explain the slower decay observed at early time. Equation (33) shows that a structured fireball yields $\alpha_2 \leq 1.92 \pm 0.18$, slightly smaller than the observed index, suggesting that collimation may also be required to accommodate the post-break decay of the this afterglow. The right panel of Figure 6 shows the best fit obtained with a structured jet interacting with a wind medium. The jet structure improves the fit by $\Delta\chi^2 = 23$ relative to the best fit obtained with a uniform jet, which is statistically significant. However, the optical light-curves steepen too slowly, overestimating the afterglow flux before and after the break and yielding $\chi^2 = 104$ for 66 df. We conclude that a wind-like medium is not compatible with the observations of the 990510 afterglow even if the jet is endowed with structure.

4.2.2. *GRB 000301c*

The R-band light-curve index of the 000301c afterglow increased from $\alpha_1 = 0.70 \pm 0.07$ to $\alpha_2 = 2.44 \pm 0.29$ (Bhargavi & Cowsik 2000), a sharp break occurring at $t \sim 4$ days (Figure 7). Jensen et al. (2001) found that, at $t = 3$ days, the optical spectral slope is $\beta_o = 0.57 \pm 0.02$ after correcting for the host reddening, determined from the curvature of the spectrum and assuming an SMC reddening law. X-ray observations were not made, thus the location of the cooling frequency is not constrained. If $\nu_c < \nu_o$ then the pre-break light-curve index (eq. [32]) $\alpha_1 = 0.36 \pm 0.03$ for a uniform outflow would be too small compared with that observed. Therefore $\nu_o < \nu_c$ seems more likely for the 000301c afterglow.

Given that structured jets interacting with a wind-like medium produce light-curves that are too smooth, we focus here only on a homogeneous circumburst medium. For $\nu_o < \nu_c$ and a uniform fireball, equation (32) yields $\alpha_1 = 0.86 \pm 0.03$, which is slightly larger than observed, thus a structured outflow is only marginally required, while equation (33) leads to $\alpha_2 \leq 1.61 \pm 0.03$, which is well below the observed value, thus a jet is required. Then, according to equation (34), $\alpha_2 = 2.14 \pm 0.04$, which is marginally compatible with the index measured by Bhargavi & Cowsik (2000). Other post-break asymptotic indices reported in the literature are larger (albeit more uncertain), which suggests that a jet model may have difficulties in explaining the steep post-break fall-off of the R-band light-curve of 000301c.

In the framework of uniform jets, we have found (Panaitescu 2001) that this indeed the case: the best fit obtained for $s = 0$ has $\chi^2 = 480$ for 98 df and $E_0 \simeq 2 \times 10^{51}$ ergs, $\Theta_0 \simeq 3\,\mathrm{deg}$, $n \simeq 0.01\,\mathrm{cm}^{-3}$, $p \simeq 2.5$, failing to produce the observed steepening $\Delta\alpha \geq 1.74 \pm 0.30$ when the jet edge becomes visible. For this reason, we have investigated a jet model where the distribution of shock-accelerated electrons has a break, so that a sharp light-curve fall-off is seen after the passage through the optical of the synchrotron characteristic frequency corresponding to this break. Further indication that the distribution of injected electrons is not a pure power-law is provided by the discrepancy between the post-break light-curve indices at radio ($\alpha_r = 1.0 \pm 0.2$) and optical frequencies, and also by the $K - R$ color change between 2 and 5 days after the burst (Rhoads & Fruchter 2001), which implies a softening of the optical spectral slope $\Delta\beta_o \lesssim 0.5$ that is too fast to be attributed to the passage of the cooling break. The best fit obtained with the broken power-law injected electron distribution has $\chi^2 = 120$ for 96 df, being marginally acceptable.

Figure 7 assesses the ability of a structured jet to accommodate the sharp break of the 000301c afterglow without recourse to a non-standard injected electron distribution. The new best fit has $\chi^2 = 204$ for 95 df, which is a substantial improvement in comparison with the uniform jet model and a pure power-law electron distribution. Nevertheless, the best fit obtained with a structured jet is not acceptable and, clearly, poorer than the uniform jet model with a broken power-law injected electron distribution. It does not reproduced well the steep post-break decay of the R-band light-curve and underestimates the 250 GHz emission. We note that, for the best fit shown in Figure 7, the cooling frequency falls within the optical domain at a few days, a feature which is required to explain the observed curvature of the optical spectrum (Jensen et al. 2001).

5. CONCLUSIONS

In the standard picture of uniform jets, the measured pre- and post-break light-curve indices and the spectral slope offer an overconstrained problem, as, for a given type of external medium, all these quantities depend only on the exponent of the power-law distribution of shock-accelerated electrons. The angular structure of GRB jets and the observer location relative to the axis of the structured jet affects the pre-break index and, possibly, the post-break index also (eq. [25]–[27], Figures 2–4). For most well-observed afterglows, a uniform jet interacting with a homogeneous external medium provides good fits (Panaitescu & Kumar 2002), indicating that the freedom allowed by the outflow structure is usually not required by current afterglow observations. Nevertheless, a simple analysis (§4.1) of the light-curve indices and spectral slopes, shows that structured outflows are required if the circumburst medium has a wind-like profile ($s = 2$), as, for such media, the resulting steep pre-break light-curve decay must be mitigated by the outflow angular structure.

Due to the slower deceleration of jets by wind-like media and the stronger sideways expansion when the jet edge becomes visible, the light-curve breaks for $s = 2$ and uniform jets are too smooth compared with the observations (Kumar & Panaitescu 2000). It is then worth investigating if an angular structure in the outflow, yielding a shallower pre-break light-curve decay, sharpens sufficiently the light-curve steepening to make it consistent with the observations. Figures 2, 3, and the right panel of Figure 6 show that the steepening of light-curves from structured fireballs/jets interacting with wind-like media lasts more than a decade in time, suggesting that such media are not able to accommodate all the observed afterglow breaks.

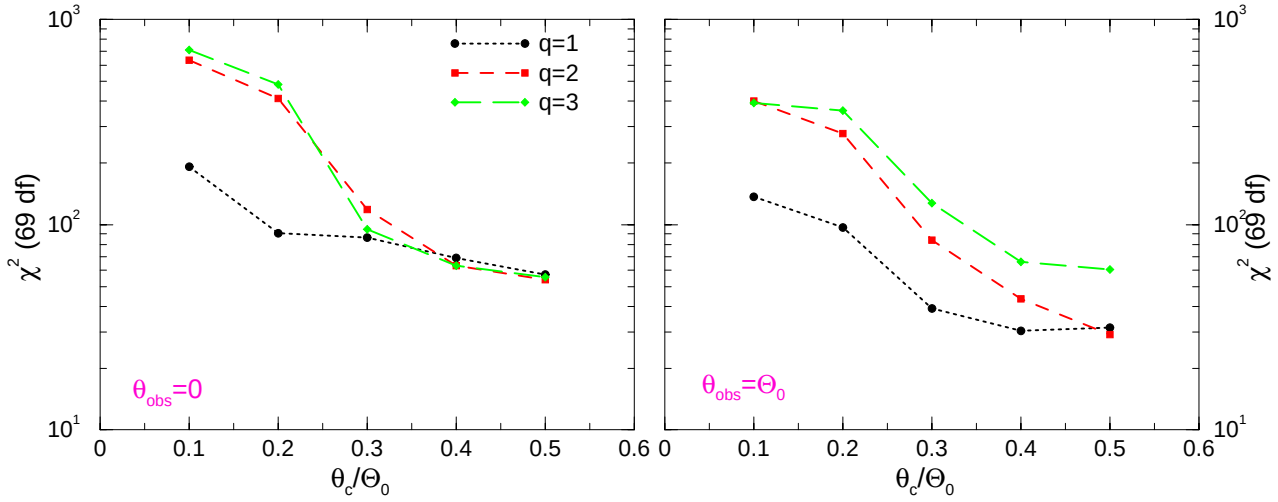

FIG. 5.— Variation of the χ^2 of the best fits to the radio, optical, and X-ray emission of the 990510 afterglow (69 degrees of freedom) with the amount of structure in the spreading jet interacting with a *homogeneous medium*. *Left panel*: observer on jet axis, *right panel*: observer on jet edge. Each point represents a combination of the ratio θ_c/Θ_0 and structural parameter q. Other model parameters (§4.2) were left free. Note that, as the angular distribution of the jet energy is more anisotropic, the fits become poorer. The best fit obtained with a uniform jet has $\chi^2 = 36$. Fits of comparable quality are obtained only if the variation of the energy per solid angle across the jet surface is less than a factor ~ 5.

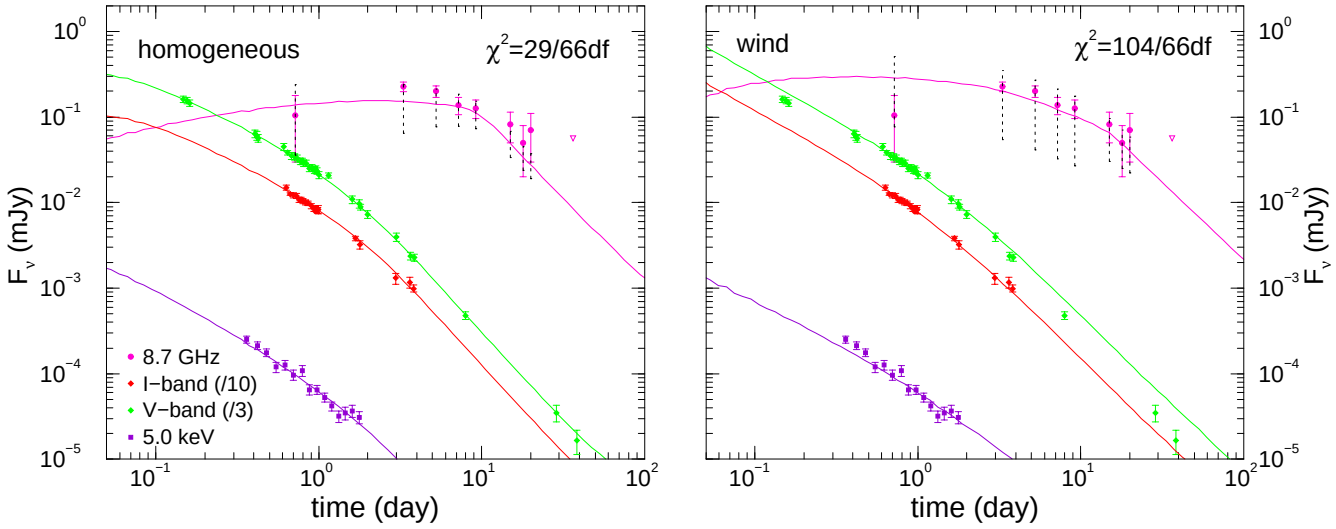

FIG. 6.— Best fits for the 990510 afterglow obtained with structured jets. *Left panel* – jet parameters are: initial energy density per solid angle along the jet axis $\mathcal{E}_0 \simeq 10^{53}$ ergs/sr, initial jet half-opening $\Theta_0 \simeq 2.2\,\theta_c$, observer location $\theta_{obs} \simeq 2.2\,\theta_c$, size of jet uniform core $\theta_c \simeq 0.8\,\mathrm{deg}$, exponent of power-law angular distribution of energy within the jet $q \simeq 1.5$ (thus the initial energy of the jet is $E_0 \simeq 2 \times 10^{50}$ ergs), electron index $p \simeq 1.8$, and *homogeneous medium* of particle density $n \simeq 0.2\,\mathrm{cm}^{-3}$, yielding $\chi^2 = 29$ for 66 degrees of freedom (df). *Right panel* – $\mathcal{E}_0 \simeq 8 \times 10^{52}$ ergs/sr, $\Theta_0 \simeq 4.6\,\theta_c$, $\theta_{obs} \simeq 1.8\,\theta_c$, $\theta_c \simeq 1\,\mathrm{deg}$, $q = 2 \div 3$ (therefore $E_0 \lesssim 3 \times 10^{50}$ ergs), $p \simeq 1.8$, and *wind-like medium* with $A_* \simeq 0.2$, yielding $\chi^2 = 104$ for 66 df. In both cases, the cooling frequency falls in the optical range, the spectral slope being in between the values given in equation (31). The vertical dotted lines indicate the amplitude of the fluctuations at 9 GHz caused by inhomogeneities in the Galactic interstellar medium. Triangles indicate $2\,\sigma$ upper limits on the 9 GHz emission. For clarity, the optical fluxes have been shifted by the factors indicated in the legend. Note that, for a wind-like medium, the steepening of the light-curve is too slow, failing to accommodate the sharpness of the break seen at 2-3 days.

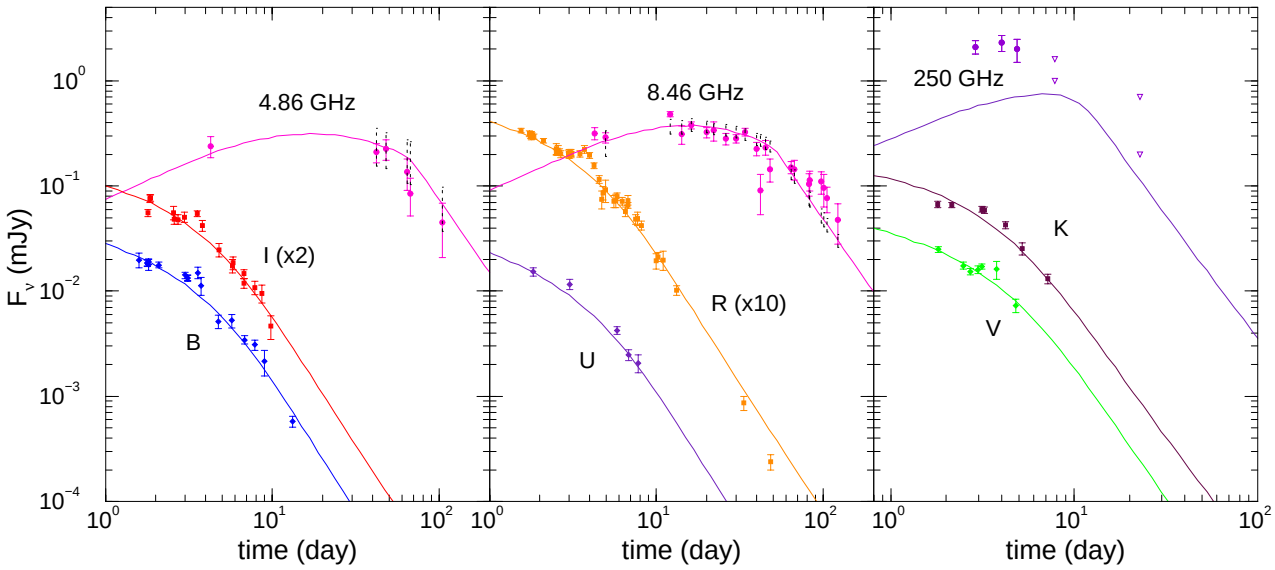

FIG. 7.— Best fit for the 000301c afterglow obtained with a structured jet and a *homogeneous external medium*. The jet parameters are $\mathcal{E}_0 \simeq 3 \times 10^{53}$ ergs/sr, $\Theta_0 \simeq 5.0\,\theta_c$, $\theta_{obs} \simeq 3.3\,\theta_c$, $\theta_c \simeq 0.8\,\mathrm{deg}$, $q \sim 3$ (therefore $E_0 \sim 5 \times 10^{50}$ ergs), $p \simeq 2.5$, and $n \simeq 0.04\,\mathrm{cm}^{-3}$. The jet energy is 4 times smaller than that obtained with a uniform jet, while the external density is 4 times larger. This fit has $\chi^2 = 204$ for 95 df, excluding the data between 3.0 and 4.3 days, when the optical light-curves exhibit a flattening, indicating a departure (e.g. delayed energy injection, clumpy external medium) from the jet model used here. Triangles indicate $1\,\sigma$ and $2\,\sigma$ upper limits on the 250 GHz emission. As for Figure 6, vertical dotted lines give the amplitude of interstellar scintillation at radio frequencies. Note the shallow decay of the model R-band emission at late times.

Using numerical calculations of the dynamics and synchrotron emission of structured jets, we find (§4.2.1) that little angular structure is allowed for the afterglow 990510 if the external medium is homogeneous. Although acceptable fits to the emission of this afterglow can be obtained even for a ten-fold variation of the kinetic energy per solid angle from its axis to edge, fits of quality comparable to that obtained with a uniform jet require an energy variation across the jet surface of less than a factor ~ 5. Allowing for structure in the jet improves significantly the best fit to 990510 obtained with a wind-like medium, nevertheless the best fit is not acceptable. The ability of structured jets to yield larger light-curve breaks was also tested against the strong steepening observed for the afterglow 000301c (§4.2.2). We find that the addition of structure greatly improves the fit obtained with a pure power-law electron distribution; however it does not fare as well as a jet model with a non-standard, broken power-law electron distribution.

Nevertheless, angular structure in a wide jet may be a viable explanation for the shallower light-curve breaks (Rossi, Lazzati & Rees 2002) seen in other GRB afterglows. In fact, as discussed in §4.1, a structured fireball is required by some afterglows if the external medium is wind-like. Evidently, the best cases for a structured outflow will be those where the light-curve indices and spectral slopes are not consistent with each other within the framework of uniform fireballs. In such cases, equations (32)–(34) and the criteria derived in §4.1 offer a simple way to assess the importance of structure and collimation in the outflow. Furthermore, equations (22), (25)–(27), and the results shown in Figure 5 can be used to constrain the angular distribution of the ejecta kinetic energy.

REFERENCES

Beuermann, K. et al. 1999, A&A 352, L26
Bhargavi, S. & Cowsik, R. 2000, ApJ 545, L77
Chevalier, R. & Li, Z.-Y. 1999, ApJ 520, L29
Dai, Z. & Gou, L. 2001, ApJ 552, 72
Frail, D. et al. 2001, ApJ 562, L55
Fynbo, J. et al. 2001, A&A 373, 796
Granot, J. et al. 2002, ApJ 570, L61
Granot, J. & Kumar, P. 2003, ApJ, submitted (astro-ph/0212540)
Harrison, F. et al. 1999, ApJ 523, L121
Jensen, B. et al. 2001, A&A 370, 909
Kardashev, N. 1962, AJ 6, no.3, 317
Kumar, P. & Panaitescu, A. 2000, ApJ 541, L9
Kuulkers, E. et al. 2000, ApJ 538, 638
Li, Z.-Y. & Chevalier, R. 2001, ApJ 551, 940
Mészáros, P., Rees, M.J. 1997, ApJ 476, 232
Mészáros, P., Rees, M.J. & Wijers, R. 1998, ApJ 499, 301
Panaitescu, A., Mészáros, P. & Rees, M.J. 1998, ApJ 503, 314
Panaitescu, A. 2001, ApJ 556, 1002
Panaitescu, A. & Kumar, P. 2002, ApJ 571, 779
Postnov, K., Prokhorov, M. & Lipunov, V. 2001, Astronomy Report 45, 236 (astro-ph/9908136)
Rhoads, J. 1999, ApJ 525, 737
Rhoads, J. & Fruchter, A. 2001, ApJ 546, 117
Rossi, E., Lazzati, D. & Rees, M.J. 2002, MNRAS 332, 945
Stanek, K. et al. 1999, ApJ 522, L39
Wei, D. & Jin, Z. 2003, A&A, submitted (astro-ph/0212514)
Zhang, B. & Mészáros, P. 2002, ApJ 571, 876